# HIV-1 Particle Production and Infectivity can be Modulated by Mutations that Affect the Stability of the Immature Gag Lattice

*Authors*
Alex B. Kleinpeter[1], Yanan Zhu[2], Donna L. Mallery[3], Sherimay D. Ablan[1], Long Chen[2,] Nathan Hardenbrook[2], Adolfo Saiardi[4], Leo C. James[3], Peijun Zhang[2,4,5], Eric O. Freed[1†]

*Affiliations*
1 Virus-Cell Interaction Section, HIV Dynamics and Replication Program, Center for Cancer Research, National Cancer Institute, Frederick, MD 21702-1201, USA
2 Division of Structural Biology, Wellcome Trust Centre for Human Genetics, University of Oxford, Oxford OX3 7BN, UK
3 MRC Laboratory of Molecular Biology, Francis Crick Avenue, Cambridge CB2 0QH, UK
4 Laboratory for Molecular Cell Biology, University College London, London, UK
5 Diamond Light Source, Harwell Science and Innovation Campus, Didcot OX11 0DE, UK
6 Chinese Academy of Medical Sciences Oxford Institute, University of Oxford, Oxford OX3 7BN, UK

† **Correspondence to**: efreed@nih.gov

**Keywords**
Human Immunodeficiency Virus-1
inositol hexakisphosphate (IP6)
HIV-1 assembly
HIV-1 maturation
maturation inhibitors

**Abstract**
The assembly of an HIV-1 particle begins with the construction of a spherical lattice composed of hexamer subunits of the Gag polyprotein. The cellular metabolite inositol hexakisphosphate (IP6) binds and stabilizes the immature Gag lattice via an interaction with the six-helix bundle (6HB), a crucial structural feature of Gag hexamers that modulates both virus assembly and infectivity. The 6HB must be stable enough to promote immature Gag lattice formation, but also flexible enough to be accessible to the viral protease, which cleaves the 6HB during particle maturation. 6HB cleavage liberates the capsid (CA) domain of Gag from the adjacent spacer peptide 1 (SP1) and IP6 from its binding site. This pool of IP6 molecules then promotes the assembly of CA into the mature conical capsid that is required for infection. Depletion of IP6 in virus-producer cells results in severe defects in assembly and infectivity of wild-type (WT) virions. Here we show that in an SP1 double mutant (M4L/T8I) with a hyperstable 6HB, IP6 can block virion infectivity by preventing CA-SP1 processing. Thus, depletion of IP6 in virus-producer cells markedly increases M4L/T8I CA-SP1 processing and infectivity. We also show that the introduction of the M4L/T8I mutations partially rescues the assembly and infectivity defects induced by IP6 depletion on WT virions, likely by increasing the affinity of the immature lattice for limiting IP6. These findings reinforce the importance of the 6HB in virus assembly, maturation, and infection and highlight the ability of IP6 to modulate 6HB stability.

## Introduction

HIV-1 virion assembly and morphogenesis rely on the assembly of a stable immature Gag lattice (hereafter referred to as the immature lattice) at the plasma membrane of virus-producing cells (reviewed in[1, 2]). This immature lattice consists of several thousand copies[3] of the HIV-1 Gag polyprotein arranged into hexameric subunits (Gag hexamers).4 The Gag polyprotein consists of four domains [matrix (MA), capsid (CA), nucleocapsid (NC), and p6] with two spacer peptides (SP1 and SP2) flanking the NC domain. The CA and SP1 domains of Gag mediate important interactions responsible for maintaining stability of Gag hexamers and therefore the stability of the immature lattice. In particular, the final few residues of the C-terminal domain of CA (CA-CTD) and SP1 fold into a six-helix bundle (6HB) that is a critical structural element in the immature lattice. The 6HB exists in a dynamic helix-coil equilibrium that facilitates both assembly of the immature lattice and subsequent events required for particle maturation and infectivity.[5, 6, 7]

HIV-1 particle maturation begins with the proteolytic processing of the Gag polyproteins in the immature lattice into their constituent domains by the viral protease (PR). The final, and rate-limiting, step in this processing cascade is the cleavage of SP1 from CA. In contrast with the other Gag cleavage sites, which are in relatively unstructured regions, the CA-SP1 junction is buried within the CA-SP1 6HB.[8, 9] The dynamic nature of the 6HB is therefore critical for allowing enough PR access to the CA-SP1 cleavage site to ensure efficient processing at that site. The removal of SP1 from CA leads to the collapse of the 6HB and immature lattice. The liberated CA proteins then assemble into the capsid, a closed, conical shell consisting of ~250 CA hexamers and 12 CA pentamers.[10] The capsid encloses the viral genome and enzymes reverse transcriptase (RT) and integrase (IN) to form a structure that is collectively referred to as the viral core. The construction of a stable core marks the completion of productive maturation, rendering the virus particle mature and infectious.

Despite its exclusive presence in the immature lattice, the CA-SP1 6HB is also a critical determinant for particle maturation and infectivity. The stability of the 6HB is inversely correlated with the efficiency of CA-SP1 processing; increased 6HB stability blocks PR access to the CA-SP1 cleavage site, resulting in a decrease in the efficiency of CA-SP1 processing and a defect in core formation and particle infectivity. Indeed, this is the mechanism that underlies the antiviral activity of maturation inhibitors (MIs), which bind inside the 6HB and hyperstabilize the immature lattice[11, 12, 13, 14, 15, 16, 17.] While MIs have not yet been approved for clinical use, the field of MI development has generated a tremendous amount of knowledge regarding the assembly and maturation of HIV-118. In particular, the study of viral resistance to MIs has helped establish the importance of the 6HB as a structural keystone during the late stages of HIV-1 replication. Certain mutations within SP1 and the major homology region (MHR) of CA acquired during propagation of HIV-1 in the presence of the MIs bevirimat (BVM) and PF-46396 (PF96) result in severe assembly and replication defects that render these mutants dependent on MIs for replication[19, 20]. Subsequent propagation of these MI-dependent mutants in the absence of MIs leads to the acquisition of a second-site compensatory mutation in SP1:T8I that also restores replication to these assembly-defective mutants. The SP1-T8I (T8I) mutation phenocopies the antiviral effect of MIs by stabilizing the 6HB and blocking CA-SP1 processing.[20] This has led to the development of a well-supported model (reviewed in18) in which 6HB stability is finely tuned to promote both assembly of the immature lattice during particle production and CA-SP1 processing during maturation. The assembly-defective mutants selected during MI treatment destabilize the 6HB, relieving the block in CA-SP1 processing, but are reliant on MIs (or the SP1-T8I mutation) for proper assembly. Indeed,

multiple studies have described MI-induced assembly of otherwise assembly-deficient mutant viruses.[19, 20, 21]

The 6HB is not only the target of MIs but is also the binding site for the HIV-1 assembly co-factor inositol hexakisphosphate (IP6), a cellular polyanionic metabolite present in human cells at ~20–60 μM.22, 23 IP6 binds the 6HB via electrostatic interactions with two lysine residues at the top of the 6HB – CA-K158 and CA-K227 (CA numbering) – each of which forms inward-facing positively charged rings at the center of Gag hexamers.[24] Numerous studies have shown that IP6 is essential for immature lattice assembly and particle production.[24, 25, 26] However, stabilization of the immature lattice is not the only critical role that IP6 plays during the HIV-1 replication cycle. IP6 is also required to bind and promote the assembly of the capsid to complete particle maturation[24, 27] and it promotes capsid stability and reverse transcription in multiple in vitro systems,[28, 29] though the importance of IP6 in target cells is less clear.[25, 30] IP6 promotes core assembly and stability by binding to and stabilizing the CA hexamers and pentamers that comprise its capsid shell.[24, 29, 31, 32] Importantly, our recent work suggests that it is the IP6 molecules that bind to the 6HB during particle production that drive core assembly in virions.[27, 33] First, we demonstrated that mutation of either lysine responsible for IP6 binding within Gag hexamers to alanine (K158A or K227A) results in severe defects in virus assembly, IP6 packaging, and virion infectivity.[27] These defects are likely due to a destabilization of the 6HB due to an inability to bind and package IP6, leading to a defect in core formation and infection. Strikingly, we found that addition of the T8I mutation (or other 6HB-stabilizing mutations such as SP1-M4L) or treatment with the MI PF96 rescued the virus assembly and virion infectivity defects exhibited by K158A and K227A mutants by restoring IP6 packaging, presumably by stabilizing the 6HB and facilitating IP6 binding via the remaining lysine ring.[27] We also showed that the T8I mutation drastically increases the efficiency of immature lattice assembly in vitro in the presence of IP6, suggesting positive cooperativity between 6HB stability and IP6 binding.[27] Subsequently, we reported that mutation of both lysines to alanine (K158A + K227A or 'KAKA') resulted in only a very mild decrease in virus production despite the inability of the KAKA mutant to recruit IP6 during immature lattice assembly. However, KAKA virions contain essentially no IP6, assemble fewer and less stable cores, and display severe defects in infectivity.[33] This led us to propose that the requirement for IP6 in particle assembly is a mechanism to ensure IP6 packaging into particles to promote capsid assembly during maturation.[33]

Here we have generated an HIV-1 Gag mutant with two amino acid substitutions in its SP1 domain (SP1-M4L and T8I), each of which independently stabilizes the 6HB. We show that combining these mutations (M4L/T8I) results in a severe defect in CA-SP1 processing and virion infectivity. Producer-cell IP6 depletion, which drastically reduces WT virion infectivity, partially restores the infectivity of M4L/T8I virions. This effect is associated with increased CA-SP1 processing. In addition, we show that the M4L/T8I mutations rescue the defects in virus assembly imposed on WT virions by producer-cell IP6 depletion. These findings demonstrate that producer-cell IP6 can serve either a proviral or antiviral role, depending on the inherent stability of the 6HB, thus highlighting the finely tuned stability of the immature Gag lattice as a property of virion morphogenesis that ensures efficient assembly, maturation, and infectivity.

## Results

*Mutants with a stabilized immature lattice display reduced sensitivity to IP6 depletion in virus-producer cells relative to WT*

In a previous study, we selected for mutations within the CA-CTD (N193H) and SP1 (M4L and T8I) upon propagation of IP6-binding-deficient HIV-1 Gag mutants (K158A or K227A) (Figure 1(A)).[27] These mutations, particularly T8I, compensate for defects in virus production, IP6 incorporation, and virion infectivity induced by the K158A and K227A mutations. Therefore, we sought to determine whether the CA-N193H, SP1-M4L, and SP1-T8I (referred to hereafter as N193H, M4L, and T8I) mutations could compensate for similar defects induced by depletion of IP6 in virus-producing cells. Recently, we and others reported that cellular IP6 could be depleted ~50 fold by overexpressing multiple inositol polyphosphate phosphatase 1 (MINPP1) in knockout cells lacking either inositol polyphosphate multikinase (IPMK KO), or inositol pentakisphosphate 2-kinase (IPPK KO), which are responsible for converting IP3/4 to IP4/5 and IP5 to IP6, respectively[25, 33] (Figure 1(B)). Conversely, MINPP1 converts IP6 to IP5, IP5 to IP4, and IP4 to IP3. Therefore, the strategy of combining MINPP1 overexpression with IPMK or IPPK KO depletes both cellular IP6 and IP5, the latter of which is also capable of facilitating HIV-1 assembly and infectivity to a lesser extent than IP6.[25, 26, 34]

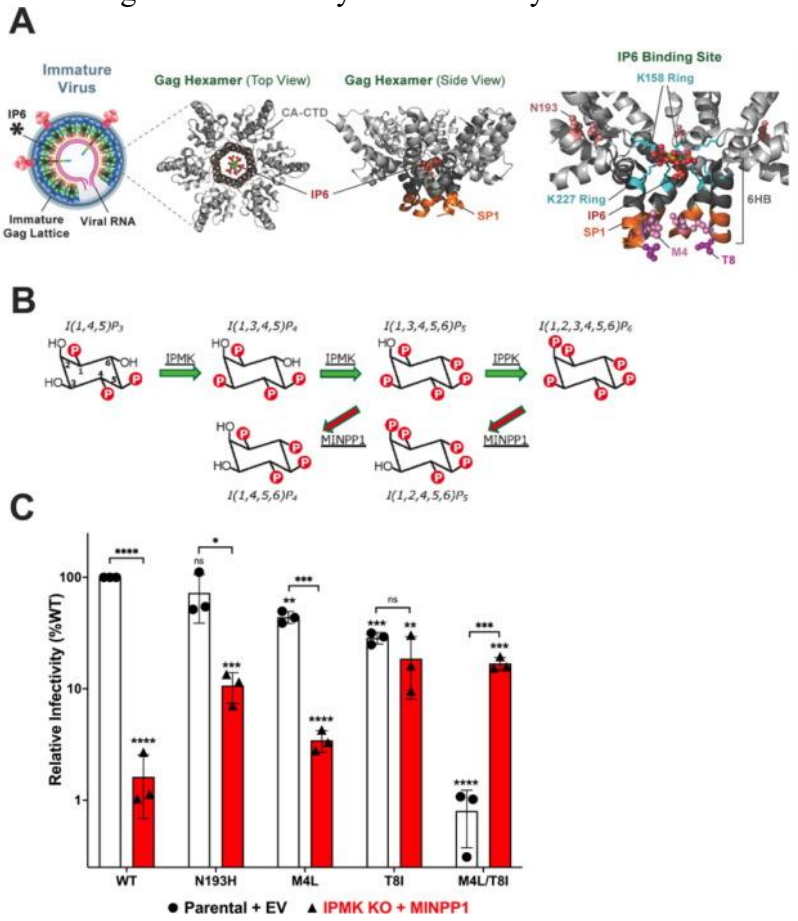


*Figure 1. 6HB-stabilizing Gag mutants show differential sensitivity to IP6 depletion in virus-producing cells. (A) IP6 binds to the center of Gag hexamers that comprise the immature Gag lattice (left). Top and side views of IP6-bound Gag hexamers (middle). Structure of the CACTD and SP1 6HB region of a Gag hexamer with location of key amino acids investigated in this study. IP6 is shown (orange) coordinated at the top of the 6HB by the Lys-158 and Lys-227 rings. The locations of CA-Asn-193 (N193), SP1-Met-4 (M4), and SP1-Thr-8 (T8) are also shown. Image modified from.[27] Models generated using PDB IDs 6BHR and 6N3U. (B) Cartoon showing the relevant biosynthetic pathways for the phosphorylation and de-phosphorylation of inositol phosphates. Image from.[33] (C) Single cycle infectivity measurements from TZM-bl cells for WT and mutant virions collected from 293T parental*

*(white bars) and IP6-depleted cells (red bars). Virions were collected after a 48-hour incubation. IP6 was depleted via co-transfection of IPMK KO cells with pNL4-3 plasmid and 500 ng MINPP1. Measurements are the mean of three independent experiments and error bars depict this mean +/- SEM. Statistical analysis was performed using GraphPad Prism. Asterisks above each bar represent level of statistical significance relative to WT in parental cells as determined by a one-sample Student's t-test with a hypothetical mean set to 100 to account for normalization. All other comparisons were made using unpaired Student's t-tests. (p-value summary: >0.05 = not significant (ns); <0.05 = *; <0.01 = **; <0.001 = ***; <0.0001 = ****).*

As we reported previously,[33] WT HIV-1 virions produced from 293T IPMK KO cells co-transfected with pNL4-3 and a MINPP1 expression construct demonstrated a marked, ~50-fold decrease in infectivity compared to virions produced in parental 293T cells co-transfected with pNL4-3 and an empty vector (EV) (Figure 1(C)). In contrast, N193H and M4L virions demonstrated ~10-fold decreases in infectivity in IP6-depleted cells compared to parental cells, whereas T8I virion infectivity was insensitive to IP6 depletion in virus-producer cells. All virion infectivity assays were performed on TZM-bl cells as described previously[27] using multiple viral inputs to ensure that normalized values fell within the linear range of infectivity (Supplementary Figure 1). Furthermore, infectivity measurements are normalized to RT activity present in viral supernatants to account for any differences in virus production and are therefore a measurement of specific infectivity. Consistent with our previous work,[27] T8I virions produced in parental cells displayed substantially decreased infectivity compared to N193H and M4L virions, which showed only mild defects compared to WT. This is also consistent with our previous results that indicate that T8I confers increased immature lattice stability compared to N193H and M4L.[27] Together, these data suggest that while increased immature lattice stability decreases virion infectivity, sensitivity to IP6 depletion is also decreased by lattice-stabilizing mutations.

*Producer-cell IP6 depletion increases M4L/T8I virion infectivity*

To further test the notion that immature-lattice-stabilizing mutations reduce sensitivity to IP6 depletion, we generated a double mutant (M4L/T8I) that would presumably stabilize the immature lattice to an even greater extent than T8I alone. Indeed, M4L/T8I demonstrated a ~100-fold defect in virion infectivity when produced in parental cells (Figure 1(C)). Strikingly, however, M4L/T8I virions produced from IP6-depleted cells displayed a ~20-fold increase in infectivity compared to particles produced from parental cells. This led us to hypothesize that IP6 depletion in producer cells destabilizes the immature lattice; in the context of a hyperstable immature lattice, such as that of M4L/T8I, IP6 depletion thus brings the stability of the immature lattice closer to that of native WT stability, partially restoring infectivity.

*IP6 depletion in producer cells restores CA-SP1 processing of mutants with a hyperstable immature lattice*

To determine the mechanism driving the defect in virion infectivity of mutants containing a hyperstable 6HB (Figure 1(C)), we examined their ability to process CA-SP1 to mature CA. We utilized our previously described35 CA-SP1 processing assay with modifications in which virus-producing cells are treated with 35S-labelled Cys and Met for 5 hours. Virus is collected, pelleted, and subjected to gel electrophoresis to separate CA (p24) from CA-SP1 (p25). CA-SP1 processing is then quantified via phosphorescence as a ratio of CA to total CA + CA-SP1. Consistent with our previous data,[20, 27, 36] we observed that the SP1-T8I mutant exhibits a defect in CA-SP1 processing, with a ratio of CA to CA + CA-SP1 of around 1:1 (50% CA-SP1 processing), in contrast to WT in which nearly 100% of CA-SP1 is cleaved to CA (Figure

2(A),Figure 2(B), white bars). The M4L/T8I double mutant displayed a ~10-fold defect in CA-SP1 processing. Combining the M4L/T8I substitutions with the KAKA mutations, which prevent IP6 binding to the 6HB,[33] led to a partial rescue of CA-SP1 processing relative to M4L/T8I alone (Figure 2(A):Figure 2(B), white bars).

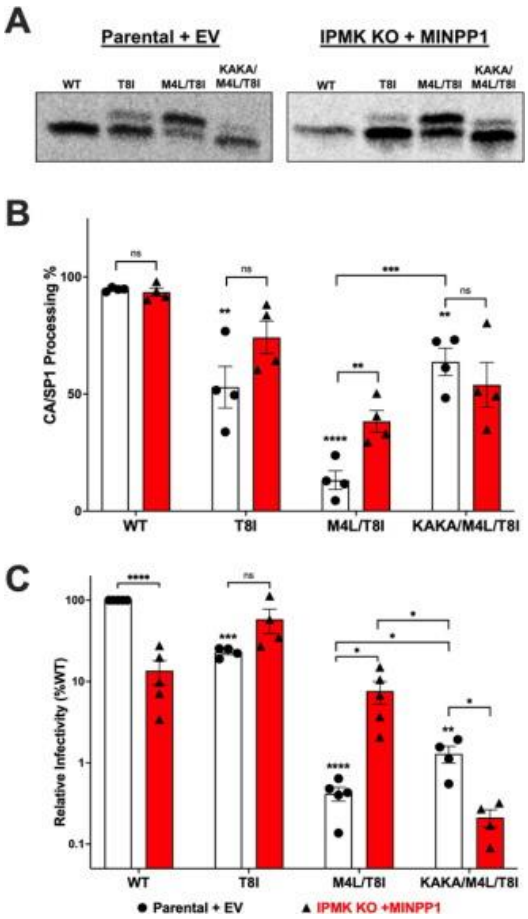


*Figure 2. IP6 depletion restores CA-SP1 processing to M4L/T8I. (A) Representative CA-SP1 processing gel imaged and quantified using 35S phosphorescence. (B) WT and mutant virions collected from 293T parental (white bars) and IP6-depleted cells (red bars) labeled with 35S. Virions were collected after a 5-hour incubation. IP6 was depleted via co-transfection of IPMK KO cells with pNL4-3 plasmid and 250 ng MINPP1. CA-SP1 processing was quantified by SDS-PAGE to separate CA (p24) and CA-SP1 (p25). (C) Single cycle infectivity experiments matched with CA-SP1 processing experiments described in (B). Virions were collected after a 5-hour incubation and infectivity was determined on TZM-bl cells. IP6 was depleted via co-transfection of IPMK KO cells with pNL4-3 plasmid and 250 ng MINPP1. Measurements are the mean of at least three independent experiments and error bars depict this mean +/- SEM. Statistical analysis was performed using GraphPad Prism. Asterisks above each bar represent level of statistical significance relative to WT in parental cells. All comparisons were made using unpaired Student's t-tests. (p-value summary: >0.05 = not significant (ns); <0.05 = *; <0.01 = **; <0.001 = ***; <0.0001 = ****).*

We next sought to test whether IP6 depletion in the virus-producer cells could affect CA-SP1 processing in the context of the 6HB-stabilizing mutants T8I and M4L/T8I. We also performed matched infectivity assays to correlate our CA-SP1 processing with virion infectivity (Figure 2(C)). For these experiments we used half of the MINPP1 expression construct in the IPMK

KO cells as the experiments described in Figure 1(C) to compensate for the shorter virus collection time (48 hours vs. 5 hours). The general trends in infectivity were the same, although IP6 depletion reduced WT virion infectivity by only ~7-fold under these conditions (Compare Figures 1(C) and 2(C)).

The CA-SP1 processing data (Figure 2(B)) are consistent with the infectivity measurements (Figure 2(C)). As expected, CA-SP1 processing of WT virions was not affected by IP6 depletion. Similarly, the difference in T8I CA-SP1 processing in parental versus IP6-depleted cells was not statistically significant. However, IP6 depletion resulted in a ~4-fold increase in CA-SP1 processing for the M4L/T8I mutant. These data strongly support the hypothesis that the mechanism underlying the increase in M4L/T8I virion infectivity observed upon IP6 depletion is at least partially a restoration of CA-SP1 processing due to a decrease in 6HB stability resulting from the loss of IP6 binding. To test this hypothesis, we coupled M4L/T8I with mutations at each of the lysine rings (K158A and K227A; KAKA) responsible for immature lattice binding to IP6 during virus assembly. Virions harboring the KAKA mutations assemble in an IP6-independent manner,[33] allowing us to directly probe the effect of the loss of IP6-mediated 6HB stability in the context of M4L/T8I. Addition of the KAKA mutations partially restores CA-SP1 processing to M4L/T8I virions produced in parental cells (Figure 2(B), white bars), suggesting that the KAKA mutations reverse the hyperstability of the M4L/T8I 6HB, likely by preventing IP6 binding to the 6HB. However, we noted that adding the KAKA mutations to M4L/T8I more effectively restores CA-SP1 processing than depleting IP6 in the context of M4L/T8I (compare M4L/T8I red bar with KAKA/M4L/T8I white bar in Figure 2(B) whereas the inverse is observed with infectivity; i.e., depleting IP6 in the context of M4L/T8I results in a greater improvement in infectivity than adding the KAKA mutations (compare M4L/T8I red bar with KAKA/M4L/T8I white bar in Figure 2(C)). This suggests that the increase in M4L/T8I virion infectivity resulting from IP6 depletion cannot be entirely explained by a restoration of CA-SP1 processing.

To confirm that the KAKA mutations prevent IP6 binding to Gag hexamers, we produced and purified WT and KAKA immature virus-like particles (VLPs) in parental 293T cells. Using cryo-electron tomography (cryo-ET), we show that KAKA VLPs assemble an immature lattice similar to that of WT VLPs (Figure 3(A) and (B)). We then used subtomogram averaging (STA) to solve the structures of the Gag hexamers that comprise the immature lattice present in each of these VLPs. As expected, the WT Gag hexamer structure, determined at a global resolution of 4.15 Å, contained a clear density present at the top of the 6HB corresponding to the IP6-binding site (Figure 3(C)). However, the KAKA mutant Gag hexamer structure, determined at a resolution of 3.59 Å, did not contain any such density (Figure 3(D)). This is consistent with our previous work showing that the KAKA mutant was unable to enrich IP6 into virions.[33] Fourier shell correlation plots are shown in Supplementary Figure 2.

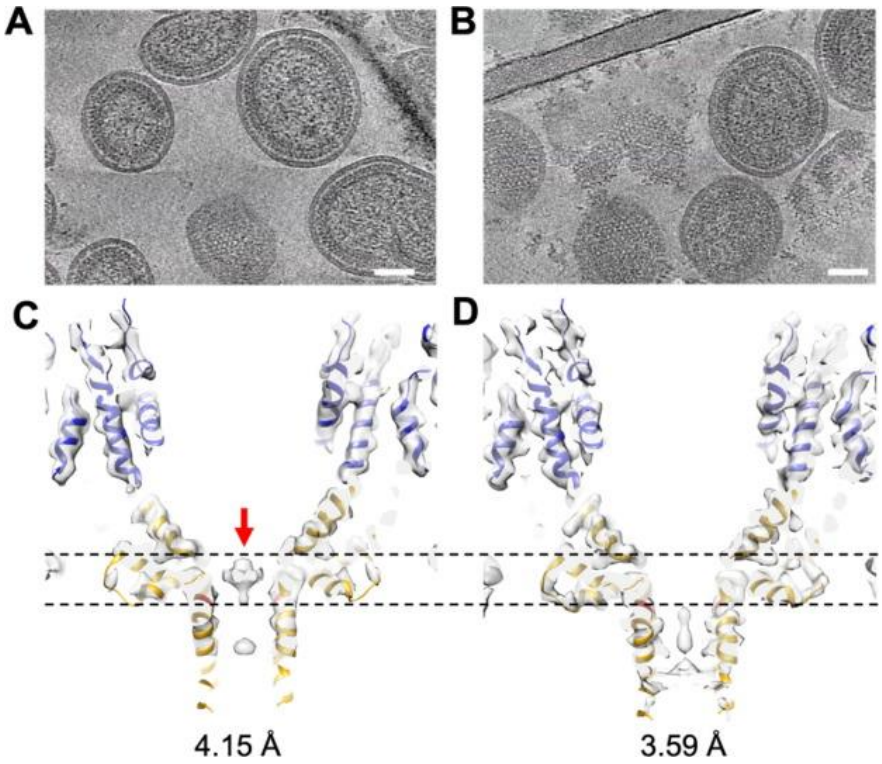


*Figure 3. CryoET and subtomogram averaging of Gag VLPs. (A-B) Tomographic slices of WT (A) and KAKA (B) Gag VLPs. (C-D) CryoET STA maps of WT (C) and KAKA (D) Gag hexamers at 4.15 Å and 3.59 Å resolution, respectively, overlapped with an immature CA-SP1 atomic model. CA-NTD and CA-CTD-SP1 are colored in blue and gold, respectively. The red arrow points to the IP6 density and the dashed lines indicate the positioning of K/A 158 and K/A 227. Scale bars, 50 nm.*

An additional contributor to the increase in infectivity of M4L/T8I virions produced in IP6-depleted cells relative to those produced in parental cells may be that the increased 6HB stability conferred by the M4L/T8I mutations increases the affinity of the immature lattice for IP6. This would result in increased IP6 packaging into M4L/T8I virions produced in IP6-depleted cells compared to WT virions under the same conditions, leading to more efficient capsid assembly during maturation. Importantly, this explanation is consistent with our previous work, which showed that T8I increases IP6-mediated assembly of immature VLPs in vitro and restored IP6 packaging into K158A mutant virions.[27]

*The effect of producer-cell IP6 depletion on virion infectivity is dose dependent*

To further understand the effect of producer-cell IP6 depletion on virion infectivity we titrated the MINPP1 expression plasmid in both IPMK KO and IPPK KO cells. As expected, the co-transfection of increasing amounts of empty vector into parental virus-producer cells does not affect the infectivity of either WT or M4L/T8I virions (Figure 4(A) and (B), left). As an increasing amount of MINPP1 expression plasmid was co-transfected into IPMK and IPPK KO cells with WT pNL4-3, WT virion infectivity decreased in a dose-dependent manner (Figure 4(A)). The effect of IP6 depletion was slightly larger in IPPK KO than IPMK KO cells, consistent with our previous work showing more complete IP6 depletion in IPPK KO compared to IPMK KO cells[33] This is also consistent with the fact that IPPK is the sole enzyme responsible for converting IP5 to IP6, whereas IPMK is the primary (but not sole) enzyme for converting IP4 to IP5. In contrast to WT, M4L/T8I virions showed a dose-dependent increase in infectivity when produced in IPMK KO cells co-transfected with increasing amounts of

MINPP1 expression vector (Figure 4(B)). Interestingly, the increase in the infectivity of M4L/T8I virions produced in IPPK KO cells did not require the co-transfection of the MINPP1 expression plasmid. Again, this is consistent with our previous studies which showed that IPPK KO more completely depletes cellular IP6 than IPMK KO.[26, 33] However, unlike WT virions, the ability of IP6 depletion to increase the infectivity of M4L/T8I virions in IPPK KO cells did not change as additional MINPP1 expression plasmid was co-transfected (Figure 3(B)). This suggests that IP6 depletion can only restore infection to M4L/T8I to a certain extent, with the effect plateauing at around 7% of the infectivity of WT virions produced in parental cells. Importantly, M4L/T8I virion infectivity in IPPK KO cells co-transfected with 500 ng of MINPP1 represents a >3-fold increase in infectivity compared to WT virions produced under the same conditions. This is consistent with the hypothesis that increased IP6 packaging into M4L/T8I virions relative to WT virions produced in IP6-depleted cells is responsible for at least a portion of the increase in M4L/T8I infectivity induced by producer-cell IP6 depletion. Because WT CA-SP1 processing is unaffected by producer-cell IP6 depletion (Figure 2(A) and (B)), the decrease in WT virion infectivity imposed by IP6 depletion is likely directly linked to reduced packaging of IP6 into virus particles and the resultant defect in capsid assembly. Therefore, the infectivity of WT virions produced from IP6-depleted cells should represent a cap for the particle infectivity of a given mutant assuming that the efficiency of IP6 packaging is equal between the WT and mutant immature lattices. Increased CA-SP1 processing of M4L/T8I virions produced from IP6-depleted cells relative to M4L/T8I virions produced from parental cells may explain part of the associated increase in infectivity that these virions display, but this cannot explain how M4L/T8I infectivity exceeds WT infectivity under the same conditions. Therefore, we propose that the increase in infectivity of M4L/T8I virions upon IP6 depletion represents a combination of increased CA-SP1 processing compared to M4L/T8I virions produced in parental cells and increased IP6 incorporation compared to WT particles produced under the same conditions. Again, this hypothesis is supported by our previous finding that 6HB stabilization either by mutation (e.g., T8I) or MI (PF96) treatment increases IP6 incorporation into K158A-mutant particles.[27]

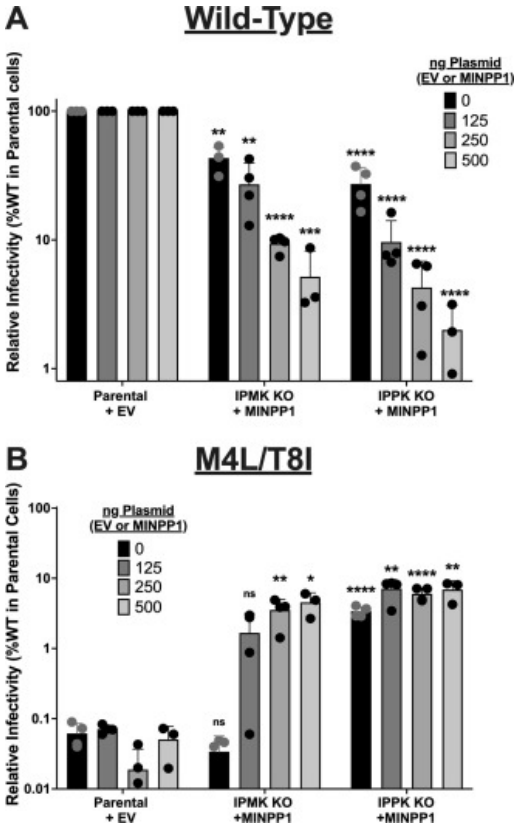


*Figure 4. The effect of producer-cell IP6 depletion on virion infectivity is dose dependent. MINPP1 expression plasmid (IPMK KO & IPPK KO cells) or empty vector (parental cells) was co-transfected with pNL4-3 WT (A) or M4L/T8I (B) plasmids at increasing levels. Virions collected after a 5-hour incubation were then assessed for single-cycle infectivity on TZM-bl cells. Infectivity was normalized to the infectivity of WT virions produced from parental cells. Measurements are the mean of at least three independent experiments and error bars depict this mean +/- SEM. Statistical analysis was performed using GraphPad Prism. Asterisks above each bar represent level of statistical significance relative to WT (A) or M4L/T8I (B) in parental cells at the appropriate amount of co-transfected empty vector. Statistical significance was determined by a one-sample Student's t-test with a hypothetical mean set to 100 to acount for normalization. (p-value summary: >0.05 = not significant (ns); <0.05 = *; <0.01 = **; <0.001 = ***; <0.0001 = ****).*

To test the hypothesis that the M4L/T8I mutant is more efficient than WT in incorporating IP6 into its 6HB, we measured the incorporation of inositol phosphates into WT and M4L/T8I virions collected from parental and IPPK KO cells supplemented with tritiated inositol. As described previously,[26, 27, 33] we used SAX-HPLC to fractionate and quantify the 3H-labeled inositol phosphates present in these virions. We were unable to utilize MINPP1 co-transfection in these experiments due to the severe decrease in virion production under these conditions. Consistent with the hypothesis that M4L/T8I increases the affinity of the immature lattice for IP6, we observed a ~1.9-fold increase in IP6 incorporation in M4L/T8I virions relative to WT virions produced from parental cells (Supplementary Figure 3(A), left). In contrast, WT and M4L/T8I virions produced in IPPK KO cells were enriched with IP5 instead of IP6, with M4L/T8I virions displaying a ~1.6-fold increase in IP5 incoroporation relative to WT virions (Supplementary Figure 3(A), right). This observation is consistent with our previous studies, which show a near-complete depletion of IP6 and an associated increase in IP5 levels in IPPK KO cells relative to parental cells.[26] Importantly, while IP6 is efficiently depleted in IPPK KO

cells, IP5 is present at sufficient levels to facilitate virus assembly and infectivity.[25] This explains the relatively modest (~3-fold) decrease in the infectivity of WT virions produced from IPPK KO cells without MINPP1 compared to the decrease in WT virion infectivity induced by MINPP1 overexpression in these cells (Figure 4(A)). In contrast, the increase in M4L/T8I infectivity in IPPK KO cells without MINPP1 relative to parental cells is similar to that observed for IPMK KO and IPPK KO cells in the context of MINPP1 overexpression (Figure 4(B)). This observation suggests that the depletion of IP6 specifically is sufficient to partially rescue the defect in M4L/T8I infectivity.

*M4L/T8I virion production and morphology are unaffected by producer-cell IP6 depletion*

The preceding results focused on the infectivity of particles produced from IP6-depleted cells. However, IP6 also plays a direct role in virus particle assembly. We therefore sought to understand the effect of producer-cell IP6 depletion on WT and M4L/T8I virion morphogenesis. We performed thin-section transmission electron microscopy (TEM) on WT and M4L/T8I virions produced from both parental and IP6-depleted cells (Figure 5). As we observed previously,[33] IPMK KO cells transfected with WT pNL4-3 showed a substantial decrease in morphologically normal particles coupled with an increase in aberrant structures compared to parental cells[33] (Figure 5(A)). These observations help to explain the decrease in the infectivity of WT virions collected from IP6-depleted cells and confirm that producer-cell IP6 depletion causes severe virion assembly defects.

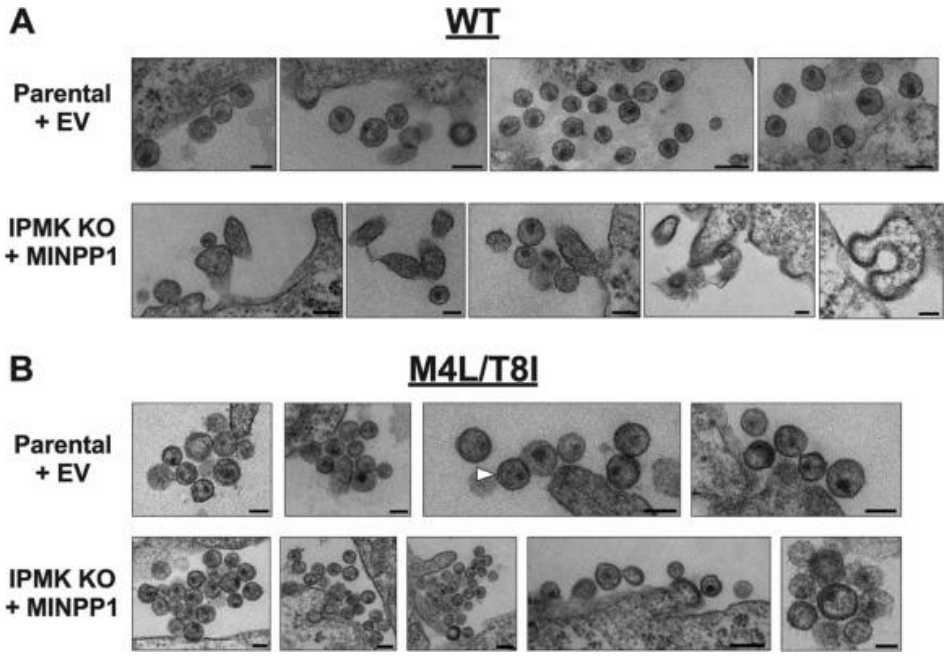


*Figure 5. M4L/T8I virion morphology is unaffected by IP6 depletion in producer cells. Thin-section transmission electron microscopy of WT and M4L/T8I virions produced in 293T parental or IP6-depleted cells (IPMK KO + MINPP1). Cells were fixed after a 24-hour incubation following media change after co-transfection of pNL4-3 plasmids with 250 ng empty vector (Parental) or MINPP1 expression construct (IPMK KO). Scale bar = 100 nm.*

M4L/T8I virions produced from parental 293T cells exhibited a morphology consistent with that previously described for both T8I and MI treatment.[12, 20, 36] This phenotype is characterized by a small crescent-shaped density of immature lattice lining the inside of the viral membrane, no clear conical core structure, and an acentric density of condensed ribonucleoprotein (Figure 5(B), white arrow). This is consistent with the severe defect in CA-SP1 processing observed in

M4L/T8I virions produced in parental cells (Figure 2(A) and (B)). Despite this defective maturation phenotype, the particles do not display any gross morphological defects. Interestingly, M4L/T8I virions produced in IP6-depleted cells are similar to those produced in parental cells (Figure 5(B)), indicating that the M4L/T8I mutations rescue the defect in virus assembly caused by producer-cell IP6 depletion (compare WT and M4L/T8I particles produced from IPMK KO + MINPP1 cells; Figure 5(A) and (B)).

We previously reported[33] that the KAKA mutant virus, like M4L/T8I, corrects the assembly defect imposed by IP6 depletion. However, the mechanisms underlying this rescue of virus assembly are presumably different for KAKA and M4L/T8I. Efficient KAKA assembly occurs in IP6-depleted cells because the KAKA immature lattice does not bind IP6 and does not require it for assembly.[33] In contrast, we hypothesize that M4L/T8I immature lattice assembly occurs efficiently in IP6-depleted cells because the increased 6HB stability conferred by these SP1 mutations compensates for the 6HB-stabilizing role that IP6 plays in assembly of the WT immature lattice, and because the highly stable M4L/T8I 6HB has a greater-than-WT affinity for the low levels of IP6 present in IP6-depleted cells. We thus sought to quantify the assembly of WT, T8I, and M4L/T8I virions in parental and IP6-depleted cells by measuring virus release efficiency. Briefly, we transfected parental and IP6-depleted cells with WT or mutant pNL4-3 molecular clones and collected cells and concentrated virus from supernatants after a 24-hour incubation. Virus production was quantified via western blot by calculating the ratio of viral CA (p24) to total Gag in the cell and virus lysate. IP6 depletion caused substantially lower levels of Gag expression in both IPMK KO and IPPK KO cells (Supplementary Figure 4). As expected, T8I and M4L/T8I viruses displayed no defects in production from parental cells compared to WT. Production of WT virus was decreased ~4–5 fold in IP6-depleted cells compared to parental cells. However, T8I and M4L/T8I virus production was either unaffected (M4L/T8I) or mildly increased (T8I) by IP6 depletion in both IPMK KO and IPPK KO cells (Figure 6(A)). These results suggest that, consistent with our TEM observations, 6HB stabilization conferred by the T8I or M4L/T8I mutations functionally restores virus production in IP6-depleted cells.

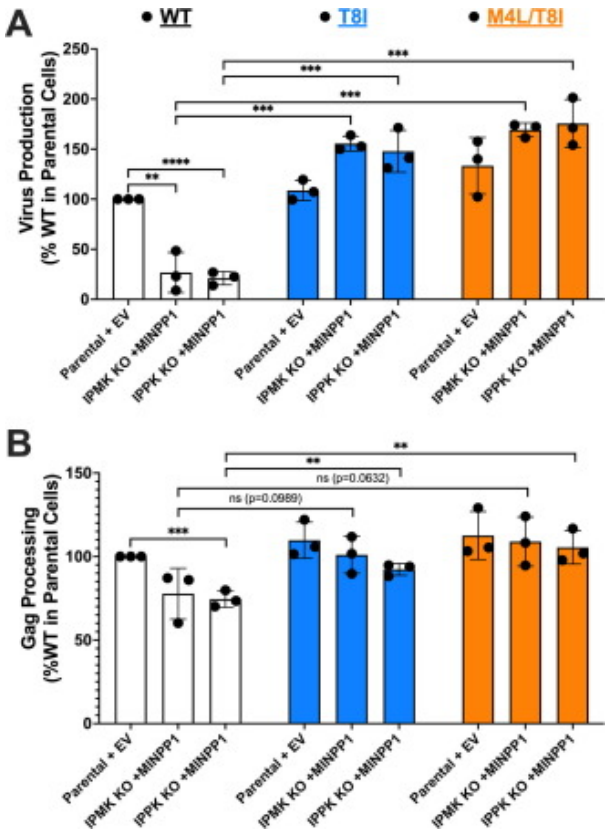


*Figure 6. 6HB-stabilizing mutations rescue defects in virus production and Gag processing induced by producer cell IP6 depletion. Cell lysates and concentrated virus lysates were collected after a 24-hour incubation following media change after co-transfection of pNL4-3 plasmids with 500 ng empty vector (Parental) or MINPP1 expression construct (IPMK KO). Cell and virus Gag levels were quantified via western blot. Measurements are the mean of three independent experiments and error bars depict this mean +/- SEM. Statistical analysis was performed using GraphPad Prism. Statistical significance was determined by a one-sample Student's t-test with a hypothetical mean set to 100 to account for normalization when comparing groups to WT in parental cells. All other comparisons were made using unpaired Student's t-tests. (p-value summary: >0.05 = not significant (ns); <0.05 = *; <0.01 = **; <0.001 = ***; <0.0001 = ****).*

We also calculated the efficiency of Gag processing for each virus in parental and IP6-depleted cells by calculating the ratio of cell-associated CA (p24) to total cell-associated Gag. While the effect size we observed was not as large as that of virus production, we did observe a decrease in WT Gag processing in IP6-depleted cells compared to parental cells. This decrease was statistically significant in IPPK KO cells. Processing of T8I and M4L/T8I Gag was not statistically different from WT in parental cells; in contrast, statistically significant increases in Gag processing were observed for T8I and M4L/T8I in IP6-depleted cells compared to WT (Figure 6(B)). While the differences observed in Gag processing are mild, this again is consistent with a defect in immature lattice assembly due to IP6 depletion that can be restored by mutations that stabilize the 6HB.

*The antiviral activity of the MI PF96 is reduced by producer-cell IP6 depletion*

Previously, we showed that 6HB-stabilizing mutations such as T8I phenocopy the effect of MI treatment by blocking CA-SP1 processing and reducing virion infectivity.[20, 27] Therefore, we sought to test the effect of MI treatment on the infectivity and CA-SP1 processing of WT

virions assembled in IP6-depleted cells. For this analysis, we used the MI PF96 at two different concentrations (5 μM and 50 μM). Consistent with previous reports,[15, 20] treatment with PF96 resulted in significantly reduced infectivity (Figure 7(A), compare white bars). As expected, reduced infectivity correlated with a decrease in CA-SP1 processing (Figure 7(B), white bars; Figure 7(C)). In contrast to the antiviral effect of PF96 on virions produced from parental cells, PF96 treatment did not result in a significant decrease in the infectivity of virions produced from IP6-depleted cells (Figure 7(A), compare red bars). Again, this is consistent with the observation that CA-SP1 processing is only mildly decreased by treatment with 5 μM PF96 and not significantly decreased by treatment with 50 μM PF96 in IP6-depleted cells (Figure 7(B), compare red bars; Figure 7(C)). Additionally, while IP6 depletion did not result in significant changes in CA-SP1 processing in the absence of PF96, PF96-treated virions displayed a statistically significant increase in CA-SP1 processing in IP6-depleted cells relative to parental cells (Figure 7(B), compare white and red bars; Figure 7(C)). This observation is consistent with our data showing that IP6 depletion increases the CA-SP1 processing of M4L/T8I. Together, these results strongly support the hypothesis that IP6 depletion destabilizes the 6HB, which, in the context of a hyperstable 6HB, results in an increase in CA-SP1 processing.

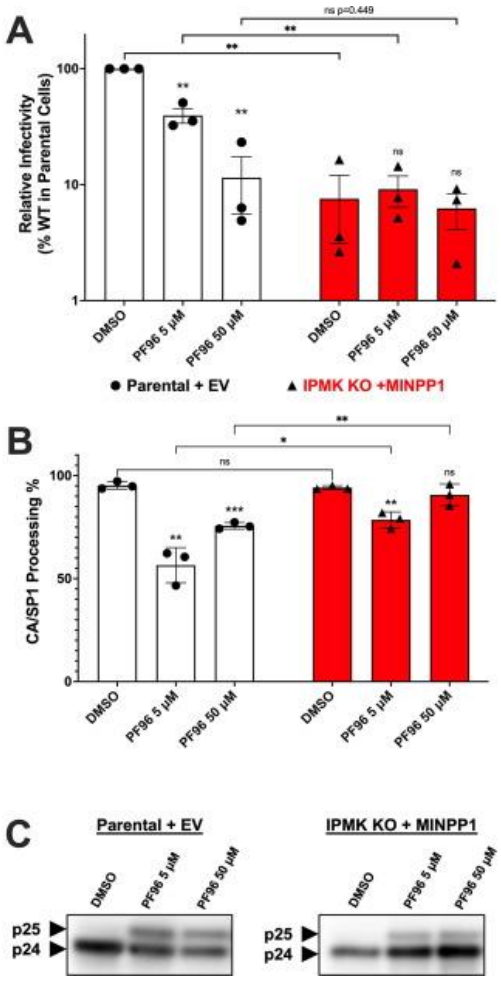


*Figure 7. MI treatment differentially affects the infectivity and CA-SP1 processing of WT virions produced from IP6-depleted cells. (A) Single cycle infectivity measurements from TZM-bl cells for WT virions collected from 293T parental (white bars) and IP6-depleted cells (red bars). Virions were collected after a 5-hour incubation and treatment with PF96 (5 μM or 50 μM) or DMSO. (B) CA-SP1 measurements calculated via western blot after a 5-hour incubation and DMSO or PF96 treatment. (C) Representative western blots for CA-SP1*

*processing. Measurements are the mean of three independent experiments and error bars depict this mean +/- SEM. Statistical analysis was performed using GraphPad Prism. Asterisks above each bar represent level of statistical significance relative to WT in parental cells as determined by a one-sample Student's t-test with a hypothetical mean set to 100 to account for normalization (white bars) or WT in IP6 depleted cells as determined by an unpaired Student's t-test (red bars). All other comparisons were made using unpaired Student's t-tests. (p-value summary: >0.05 = not significant (ns); <0.05 = *; <0.01 = **; <0.001 = ***; <0.0001 = ****).*

**Discussion**

In this study, we expand upon our previous findings to generate new insights into the role of IP6 in virion morphogenesis and infectivity. We confirm that IP6 depletion in producer cells causes a severe, dose-dependent defect in the infectivity of WT HIV-1 virions. We show that increasing the stability of the 6HB in the immature lattice via either 6HB mutations or treatment with MIs reduces sensitivity to producer-cell IP6 depletion. Most strikingly, we report a Gag mutant (M4L/T8I) that undergoes a ~20-fold increase in virion infectivity when produced from IP6-depleted cells. We also show that 6HB stabilization rescues virus assembly defects induced by producer-cell IP6 depletion. Our data extend the model describing 6HB stability as a critical determinant for particle assembly, maturation, and infectivity. Capsid formation, and therefore virion infectivity, requires both efficient CA-SP1 processing and IP6 incorporation. IP6 stabilizes the 6HB, promoting assembly of the immature lattice and virion production while simultaneously ensuring IP6 incorporation for efficient capsid assembly, core formation, and virion infectivity. However, hyper-stabilization of the 6HB blocks CA-SP1 processing, resulting in a defect in capsid formation and virion infectivity. Therefore, efficient maturation and infectivity are dependent on proper immature lattice formation during assembly with the 6HB directly or indirectly regulating each process. This argues for the development of dual-acting MIs that both block CA-SP1 processing and prevent the incorporation of IP6 into virus particles.

The most striking finding of our study is that IP6 depletion increases the infectivity of M4L/T8I virions (Figures 1(C) and 2(A)). There are two mechanisms underlying this observation. The first, and more straightforward, is that depletion of producer-cell IP6 partially restores CA-SP1 processing to M4L/T8I virions. Under normal conditions, M4L/T8I virions display an extremely severe (>100-fold) defect (Figure 2(C)) in infectivity due to an almost complete lack in CA-SP1 processing (Figure 2(A) and (B)). Production of M4L/T8I virions in IP6-depleted cells partially reverses this defect, thereby increasing infectivity. We propose that this is due to a decrease in 6HB stability imposed by a decrease in IP6 available to bind and stabilize the immature lattice. This destabilization of the hyperstable M4L/T8I 6HB re-establishes an overall stability to the immature lattice that is closer to its native WT level, resulting in increased CA-SP1 processing and particle infectivity. The second mechanism is that 6HB stabilization increases the affinity of the immature lattice for limiting IP6. We hypothesize that 6HB stabilization via T8I or M4L/T8I mutations decreases virion sensitivity to producer-cell IP6 depletion because the more stable 6HBs are better able to package IP6 than the WT 6HB. If producer-cell IP6 levels are limiting for virion infectivity, how could the infectivity of 6HB-stabilized mutant virions produced from IP6-depleted cells exceed the infectivity of WT viruses produced under the same conditions, as is the case for M4L/T8I (Figure 1(C) & 4(B))? We propose that 6HB-stabilizing mutations increase the affinity of the 6HB for limiting IP6, leading to increased IP6 incorporation into virions and more efficient capsid formation and infectivity. Although MINPP1 transfection of IPMK and IPPK KO cells drastically reduces cellular pools of IP5 and IP6, our recent work has shown that this reduction is not complete,

even at the highest levels of MINPP1 that we used in our titration experiments. Furthermore, we have shown that targeting MINPP1 to the plasma membrane more efficiently blocks HIV production and infectivity compared to the natural localization of this enzyme in the ER.[33] In the present study, we used a standard ER-localized MINPP1 expression construct, suggesting that some IP5/IP6 is available to promote particle assembly even in IPMK/IPPK KO cells expressing MINPP1. We propose that it is this IP6 that M4L/T8I more effectively binds and incorporates into its immature lattice. Additionally, this may explain why increasing levels of MINPP1 did not eventually reduce M4L/T8I infectivity.

The explanation that the M4L/T8I mutations increase the affinity of the 6HB for limiting IP6 is also consistent with our previous findings that T8I drastically increases the ability of recombinant CA-SP1 protein to assemble into VLPs in vitro and increases IP6 incorporation into K158A virions.[27] Here, we addressed this possibility by adding the KAKA mutations, which prevent IP6's interaction with the immature lattice,[33] to M4L/T8I. Despite a rescue of the CA-SP1 processing defect similar to that induced by producer-cell IP6 depletion, the addition of the KAKA mutations did not restore infectivity to M4L/T8I virions produced from parental cells to the same extent. Furthermore, the introduction of the KAKA mutations into M4L/T8I reverses the effect of producer-cell IP6 depletion such that KAKA/M4L/T8I infectivity is reduced rather than restored (Figure 2(C)). These observations suggest that the increase in M4L/T8I virion infectivity resulting from IP6 depletion is dependent on the presence of the two lysines required to bind IP6. However, we acknowledge the possibility that the KAKA mutations confer an undetermined effect that may confound these interpretations.

The hypothesis that lattice-stabilizing mutations increase the affinity of the 6HB for limiting IP6, restoring IP6 incorporation, capsid assembly, and infectivity raises the question of how the depletion of producer-cell IP6 could simultaneously decrease the stability of the M4L/T8I 6HB (due to lack of IP6 binding) to correct the CA-SP1 processing defect, and result in more efficient IP6 packaging into M4L/T8I virions than in WT virions produced in IP6-depleted cells. First, each defect should be considered independently. M4L/T8I virions produced from normal cells incorporate sufficient IP6 but suffer from a lack of liberated CA protein due to the defect CA-SP1 processing (Figure 8, green). In contrast, WT virions produced from IP6-depleted cells efficiently process CA-SP1 to CA, but do not incorporate sufficient levels of IP6 to stabilize CA hexamers during capsid assembly (Figure 8, yellow). Therefore, one possible explanation is that the immature lattice for a given M4L/T8I virion produced from IP6-depleted cells is composed of a mixture of both IP6-bound and non-IP6-bound Gag hexamers. The IP6-bound Gag hexamers incorporate IP6 into the particle for capsid assembly but are too stable to undergo CA-SP1 processing. The non-IP6-bound hexamers are incorporated into the immature lattice during assembly due to the increased stability conferred by the M4L/T8I mutations and the neighboring IP6-bound hexamers. However, the destabilizing effect of the non-IP6-bound K158 and K227 rings results in enough PR access to allow efficient CA-SP1 processing. As a result, some M4L/T8I particles contain enough CA and IP6 to permit the assembly of a stable capsid (Figure 8, dotted lines).

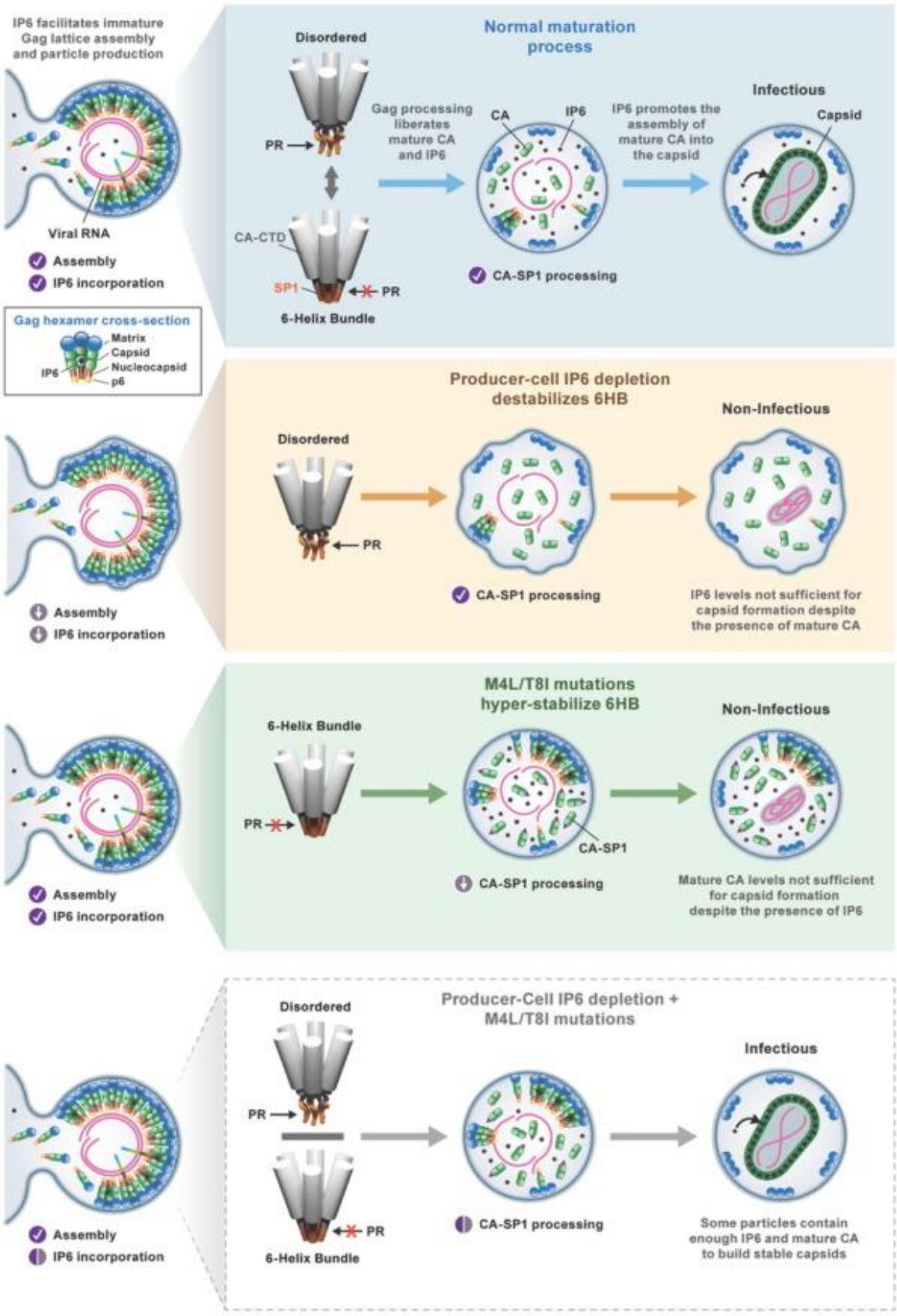


*Figure 8. Proposed model for the effect of producer-cell IP6 depletion and M4L/T8I mutations on virion infectivity. (First panel, blue) The normal HIV-1 assembly and maturation process*

*begins with the assembly of the immature Gag lattice at the plasma membrane of virus-producer cells. The CA-SP1 boundary region of Gag hexamers exists in a dynamic equilibrium between a disordered state and a stable six-helix bundle. IP6 stabilizes and promotes the assembly of the immature lattice, functionally enriching virus particles with IP6. Gag processing then liberates the packaged IP6 from its binding site and mature CA from SP1. IP6 and mature CA then assemble into the capsid, which encloses the viral genome, rendering the particle mature and infectious. (Second panel, yellow) IP6 depletion in virus-producer cells destabilizes the CA-SP1 boundary resulting in assembly defects and the production of morphologically aberrant particles lacking IP6. CA-SP1 processing proceeds normally, but without IP6, capsids do not assemble, leading to defects in virion infectivity. (Third panel, green) The M4L/T8I mutations hyper-stabilize the 6HB leading to efficient immature particle assembly and IP6 enrichment. However, the hyperstable 6HB blocks access to the viral protease (PR) resulting in inefficient CA-SP1 processing. The lack of sufficient mature CA protein prevents capsid assembly despite the presence of IP6, leading to defects in virion infectivity. (Fourth panel, dotted lines) The M4L/T8I mutations rescue the assembly defects induced by producer cell IP6 depletion by increasing the affinity of the Gag hexamers for limiting IP6. In contrast, IP6 depletion destabilizes the hyperstable M4L/T8I 6HB due insufficient IP6 binding. This results in an immature Gag lattice containing a mixture of IP6-bound hyperstable Gag hexamers, and destabilized Gag hexamers lacking IP6. The hyperstable Gag hexamers incorporate IP6, but do not undergo efficient CA-SP1 processing. In contrast, the destabilized Gag hexamers do not contribute to IP6 incorporation but undergo efficient CA-SP1 processing. During maturation, this results in intermediate levels of both mature CA and IP6 relative to WT virions produced from parental cells. Some virions contain enough IP6 and mature CA to build stable capsids, resulting in infectious particles.*

An alternative hypothesis that could explain our observations is that the assembly defect imposed on WT virions by producer-cell IP6 depletion causes defects in virion infectivity that exceed the effect of a lack of IP6 packaging. Indeed, we observed that WT particles produced from IP6-depleted cells display severe morphological defects that are corrected by 6HB-stabilizing mutations (Figure 5). All of our infectivity measurements are normalized to RT activity in the filtered supernatants that we collect. Therefore, our RT measurements for particle normalization may include RT activity from these aberrant structures that are not likely to be infectious even in the event of efficient IP6 incorporation. However, it is notable that KAKA-mutant virions produced in parental cells, which assemble efficiently despite an inability to bind and incorporate IP6 into their immature lattice, display similar levels of infectivity relative to WT virions produced from IP6-depleted cells.[33] Furthermore, the KAKA mutations also reverse the severe assembly defects observed in WT virions produced from IP6-depleted cells without restoring the defect in infectivity.[33] For these reasons, we favor the notion that the 6HB-stabilizing mutations restore infectivity to virions produced from IP6-depleted cells by increasing the affinity of the immature lattice for IP6.

Taken together, our findings demonstrate a complex role for the immature lattice, and more specifically the CA-SP1 6HB, in regulating the infectivity of HIV-1 virions. The critical role for IP6 during both assembly and maturation strengthens the fundamental link between these two processes and suggests that HIV-1 has evolved to ensure the packaging of this co-factor into virions. Ongoing studies will seek to address the crucial interplay between IP6-mediated immature lattice assembly, 6HB stability, CA-SP1 processing, and IP6 incorporation in even greater detail. Importantly, these studies will utilize the KAKA and M4L/T8I HIV-1 Gag mutants that we have generated here and elsewhere[33] as tools to study immature Gag lattice assembly and 6HB stability. Each mutant confers unique assembly phenotypes to the immature

lattice related to IP6 binding with KAKA promoting IP6-independent assembly and M4L/T8I increasing the affinity of the 6HB for IP6. These mutants will therefore be useful tools in studies aimed at expanding our understanding of the role of IP6 during HIV-1 assembly, maturation, and infection.

## Materials and methods

### *Cells and plasmids*

Human embryonic kidney (HEK) 293T parental, IPMK KO, and IPPK KO cell lines used for all experiments were the same as described in.[26, 33] TZM-bl cells (HeLa) were used for infectivity experiments.37 All cells were originally acquired from American Type Culture Collection (ATCC) and cultured in Dulbecco's modified Eagle medium (DMEM) supplemented with 10% Fetal Bovine Serum (FBS), 2 mM L-glutamine, penicillin (100 U/ml) Streptomycin (100 U/ml) at 37 °C and 5% CO2. The HIV-1 subtype B infectious molecular clone pNL4-3 was used to produce virus for all experiments. CA and SP1 mutants were generated using the New England Biolabs (NEB) Q5 site-directed mutagenesis kit (NEB E0554) using primers previously reported in27 or by direct cloning of DNA fragments acquired from GENEWIZ/Azenta. The pcDNA3 MINPP1 vector used to co-transfect IPMK KO and IPPK KO cells and pUC19 empty vector used to co-transfect parental cells are described in [33]. pNL4-3 ΔPolΔEnv constructs used for VLP production are described in [38].

### *Transfections*

All transfections were performed in 6-well plates. Briefly, cells were plated the day prior to transfection at ∼1 × 106 cells per well. On the day of the transfection, media were replaced with DMEM culture media lacking antibiotics. Transfections were carried out using 2 μg of WT or mutant pNL4-3 infectious molecular clones with 0–500 ng empty vector (Parental cells) or MINPP1 expression vector. The transfection reagent used was 1 mg/ml linear PEI (Polysciences Inc. 23966) at a 7.5(μl PEI):1(μg plasmid) ratio. Transfection media were replaced with culture media 6–18 hours post-transfection. Virus supernatants, virus lysates and/or cell lysates were harvested after a 5-hour (infectivity/CA-SP1 processing; Figure 2, Figure 4; Figure 6, Figure 7), 24-hour (virus production; Figure 6), or 48-hour (infectivity; Figure 1(C)) incubation. Virus supernatants were stored at −80 °C and virus and cell lysates were stored at −20 °C. PF96 dissolved in DMSO was added to culture media during these incubations at the indicated concentrations.

### *Single-cycle infectivity assays*

Virus supernatants were harvested from transfected parental or IP6-depleted cells and filtered through a 0.45 μm syringe filter and quantified using a 32P-based RT assay as described previously[39] and RT activity was used to normalize viral input for infectivity assays. Serial dilutions of viral stocks were made in black 96-well plates and 2 × 105 TZM-bl cells were added to each well in culture media containing 20 μg/ml DEAE-dextran (final concentration 10 μg/ml). Cells were incubated for 36–48 hours, lysed in 50 μl BriteLite reagent, and luminescence was measured using a Promega GloMax Navigator luminometer. Infectivity measurements within the linear range of detection were normalized and expressed as a percentage of the infectivity of WT virions produced in parental cells. The outer 36 wells were not used for infectivity measurements and instead filled with phosphate buffered saline (PBS) to reduce edge-effects.

### *Virus production assays*

Virus production was quantified using virus release assays as described previously.[40] Briefly, HEK293T Parental, IPMK KO, and IPPK KO cells were co-transfected with pNL4-3 WT or

mutant plasmids along with empty vector or MINPP1 expression plasmid. After a 24-hour incubation, viral supernatants were filtered and pelleted by ultracentrifugation at 4 °C. Virus pellets and cells were lysed in lysis buffer (50 mM Tris-HCl pH 7.5, 300 mM NaCl, 0.5% Triton X-100, 10 mM Iodoacetamide) supplemented with EDTA and HALT Protease and Phosphatase Inhibitor cocktail (ThermoFisher Scientific 78440). Lysates were then probed for Gag via western blot analysis. SDS-PAGE was performed using precast TGX Criterion 4–20% polyacrylamide gels (BioRad 5671094) and gels were transferred onto PVDF membranes using the BioRad Trans-Blot Turbo transfer system. Membranes were blocked for 1 hour at room temperature in 5% non-fat milk in Tris-buffered saline + 0.05% Tween 20 (TBST) and probed for Gag using the HIV-immunoglobulin (Ig) [National Institutes of Health (NIH) AIDS Reagent Program (ARP) catalog #3957] diluted 1:10000 in TBST as the primary antibody overnight. An anti-human IgG horseradish peroxidase (HRP)-tagged antibody (Sigma-Aldrich GAENA933) diluted at 1:10000 was used as the secondary antibody for 30 minutes at room temperature. SuperSignal West Pico PLUS (ThermoFisher Scientific 34578) was used as the chemiluminescent substrate. Imaging and band quantification were performed using the Sapphire Biomolecular Imager and Azure Spot analysis software (Azure Biosystems). Virus release was calculated using the formula below and normalized to WT produced in parental cells.

*CA-SP1 processing*

CA-SP1 processing was quantified by one of two methods. For the PF96 experiments (Figure 7), concentrated virus lysates collected after a 5-hour incubation were subjected to western blot analysis as described above using 12% Bis-Tris XT Criterion gels (BioRad 3450118). For the experiments in Figure 2, we used our previously described 35S-based CA-SP1 processing assay with modification.[35, 41] Briefly, transfected HEK293T parental and IP6-depleted cells were starved for 30 minutes using Roswell Park Memorial Institute 1640 medium lacking methionine (Met) and cysteine (Cys) (Sigma R7513). 35S-labeled Met and Cys were then added along with 2% dialyzed FBS (Sigma F3092) and cells were labeled for 5 hours. Concentrated virus was collected by ultracentrifugation and virus pellets were lysed as described above. Viral lysates were subjected to SDS-PAGE (12% polyacrylamide) and CA and CA-SP1 bands were visualized and quantified using phosphorescence. In both assays, CA-SP1 processing was expressed as the percentage of CA compared to total CA and CA-SP1.

*Purification and quantification of inositol phosphates*

WT and M4L/T8I particles were produced from 293T parental and IPPK KO cells cultured in inositol-free media supplemented with [3H] inositol (5 μCi/mL). After ultracentrifugation, [3H]-labelled virions were resuspended in 1 M Perchloric acid, 5 mM EDTA and incubated for 10 minutes at 95 °C and then returned to ice. Insoluble material was spun out and the supernatant was neutralized by addition of potassium carbonate and left on ice overnight. The resulting material was centrifuged for 5 minutes at 4 °C and the supernatant was used for further analysis. Inositol phosphates were resolved by strong anion exchange chromatography (SAX-HPLC) on a PArtisphere SAX 4.6° - 125 mm column (Hichrom). 1 mL fractions were collected and analyzed by scintillation counting after adding 4 mL of Ultima-Flo AP cocktail (Perkin Elmer, catalog #6013599). Disintegrations per minute (DPM) of IP4, IP5, and IP6 were normalized first to a ΔGag control to account for background counts and vesicles, and subsequently to virus yield as determined by RT ELISA.

*Thin section transmission electron microscopy (TEM)*

HEK293T parental and IPMK KO cells were transfected with WT or mutant pNL4-3 along with an empty vector (parental cells) or MINPP1 (IPMK KO cells). Fixation of cells, preparation of samples, and TEM were performed as previously described.[40]

*Virus-like particle production for CryoET analysis*
1.5 × 107 HEK293T cells were seeded in T-225 flasks and transfected as described above with WT and KAKA pNL4-3 ΔPolΔEnv constructs to produce immature VLPs. Virus supernatant was harvested at 48 hours post-transfection, centrifuged to remove cell debris, and filtered through a 0.2 μm-syringe filter. Filtered supernatants were then pelleted by ultracentrifugation (100,000 × g at 4 °C for 1 hour) in an Sorvall AH629 rotor (through an 8% iodixanol cushion). VLPs were then resuspended in PBS and ultracentrifuged (120,000 × g at 4 °C for 2.5 hours) through a 30–10% iodixanol gradient in a Sorvall TH-660 rotor. The virus-containing fraction was then diluted 1:8 in PBS and concentrated by ultracentrifugation (110,000 × g at 4 °C for 2 hours). VLP pellets were resuspended in PBS and incubated at 4 °C overnight to allow full resuspension.

*CryoET and subtomogram averaging*
CryoET tilt series were acquired in eBIC (Electron BioImaging Centre, Diamond) using a Thermo Fisher Titan Krios microscope operated at 300 keV equipped with a Gatan Quantum post-column energy filter (Gatan Inc) operated in zero-loss mode with 20 eV slit width and a Gatan K3 direct electron detector at a nominal magnification of 64k and a physical pixel size of 1.34 Å per pixel. Data were collected automatically using the SerialEM software[42] and a dose-symmetric tilt-scheme[43] with a 3° tilt increment and an angular range of ±60°. The accumulated dose of each tilt series was ∼123 e−/Å2 and the defocus range was −1.5 to −6 μm. In total, 41 tilt series from the wild type Gag VLPs and 71 tilt series from KAKA Gag VLPs were collected. Each projection image was dose-fractioned into ten frames. Details of data collection parameters are listed in Supplementary Table 1.
An automated cryoET processing pipeline (https://github.com/ffyr2w/cet_toolbox) was used for motion correction[44] of the raw frames and tilt-series alignment with IMOD.[45] The fiducial markers were manually inspected to ensure the centering of markers for each tilt series in eTOMO. Subtomogram averaging for both datasets was performed following the workflow of emClarity.[46, 47] The HIV-1 Gag structure (EMD-8403)[48] was low-pass filtered to 30 Å and used as the initial reference for template search in 6x binned tomograms with a pixel size of 8.06 Å. 114,401 subtomograms were selected from 41 tilt series for the wild type dataset and 122,575 subtomograms were selected from 71 tilt series for the KAKA Gag VLP dataset. The subtomogram averaging and alignment were performed iteratively using 6x, 5x, 4x, 3x, 2x, and 1x binned tomograms. A cylindrical alignment mask including 7 hexamers was used for initial alignment and a 6-fold symmetry was applied throughout the alignment procedure. The final density maps were reconstructed at bin 1 and sharpened with a b-factor of −50.

**Data and materials availability**
The cryoET STA maps of the wild type and KAKA mutant Gag VLPs have been deposited in EMDB under accession code EMD-16187 and EMD-16190, respectively.

**Authorship contribution statement**

Alex B. Kleinpeter: Conceptualization, Methodology, Formal analysis, Investigation, Writing – original draft, Visualization, Project administration. Yanan Zhu: Methodology, Software, Formal analysis, Investigation, Writing – review & editing, Visualization. Donna L. Mallery: Formal analysis, Investigation, Writing – review & editing. Sherimay D. Ablan: Formal

analysis, Investigation, Writing – review & editing. Long Chen: Software, Formal analysis, Investigation, Writing – review & editing. Nathan Hardenbrook: Software, Formal analysis, Investigation, Writing – review & editing. Adolfo Saiardi: Methodology, Formal analysis, Writing – review & editing. Leo C. James: Supervision, Writing – review & editing, Funding acquisition. Peijun Zhang: Supervision, Writing – review & editing, Funding acquisition. Eric O. Freed: Conceptualization, Supervision, Writing – review & editing, Funding acquisition.

**Acknowledgements**
This research was supported by the Intramural Research Program of the Center for Cancer Research, National Cancer Institute, National Institutes of Health. ABK was supported in part by an Intramural AIDS Research Fellowship. Work in the James laboratory was supported by the MRC (UK; U105181010), a Wellcome Trust Investigator Award (223054/Z/21/Z), and a Wellcome Trust Collaborator Award (214344/A/18/Z). Work in the Zhang lab was supported by the National Institutes of Health P50 grant (AI150481), the UK Wellcome Trust Investigator Award (206422/Z/17/Z), and the UK Biotechnology and Biological Sciences Research Council grant (BB/S003339/1). The Saiardi Laboratory was supported by the MRC (UK Grant MR/T028904/1). We are grateful to the Center for Cancer Research Electron Microscopy Lab, (EML), particularly Ferri Soheilian and Steven Felkowski for TEM imaging. We are also grateful to Clayton Smith (National Cancer Institute Cryo-EM Facility at the Frederick National Laboratory for Cancer Research) for assistance in Cryo-EM/ET grid preparation. We acknowledge Diamond Light Source for access and support of the cryoEM facilities at the UK National Electron Bio-imaging Center (eBIC, proposal NT29812), funded by the Wellcome Trust, MRC, and BBSRC. We thank Yun Song for technical support on cryoET data collection. We thank Brian Luke (Bioinformatics and Computational Science Program at NCI-Frederick) for advice regarding statistical analysis.

**Declaration of Competing Interest**
The authors declare that they have no known competing financial interests or personal relationships that could have appeared to influence the work reported in this paper.

**References**


1 E.O. Freed
HIV-1 assembly, release and maturation
Nat. Rev. Microbiol., 13 (2015), pp. 484-496

2 G. Lerner, N. Weaver, B. Anokhin, P. Spearman
Advances in HIV-1 Assembly
Viruses, 14 (2022), p. 478

3 J.A. Briggs, M.N. Simon, I. Gross, H.G. Kräusslich, S.D. Fuller, V.M. Vogt, et al.
The stoichiometry of Gag protein in HIV-1
Nat. Struct. Mol. Biol., 11 (2004), pp. 672-675

4 C.L. Ricaña, R.A. Dick
Inositol Phosphates and Retroviral Assembly: A Cellular Perspective
Viruses, 13 (2021), p. 2516

5 M. Wang, C.M. Quinn, J.R. Perilla, H. Zhang, R. Shirra Jr., G. Hou, et al.
Quenching protein dynamics interferes with HIV capsid maturation
Nat. Commun., 8 (2017), p. 1779

6 L. Mendonça, D. Sun, J. Ning, J. Liu, A. Kotecha, M. Olek, et al.
CryoET structures of immature HIV Gag reveal six-helix bundle
Commun. Biol., 4 (2021), p. 481

7 T.A. Bharat, L.R. Castillo Menendez, W.J. Hagen, V. Lux, S. Igonet, M. Schorb, et al.
Cryo-electron microscopy of tubular arrays of HIV-1 Gag resolves structures essential for immature virus assembly
PNAS, 111 (2014), pp. 8233-8238

8 F.K. Schur, M. Obr, W.J. Hagen, W. Wan, A.J. Jakobi, J.M. Kirkpatrick, et al.
An atomic model of HIV-1 capsid-SP1 reveals structures regulating assembly and maturation
Science, 353 (2016), pp. 506-508

9 J.M. Wagner, K.K. Zadrozny, J. Chrustowicz, M.D. Purdy, M. Yeager, B.K. Ganser-Pornillos, et al.
Crystal structure of an HIV assembly and maturation switch
Elife, 5 (2016)

10 G. Zhao, J.R. Perilla, E.L. Yufenyuy, X. Meng, B. Chen, J. Ning, et al.
Mature HIV-1 capsid structure by cryo-electron microscopy and all-atom molecular dynamics
Nature, 497 (2013), pp. 643-646

11 S. Gupta, J.M. Louis, R. Tycko
Effects of an HIV-1 maturation inhibitor on the structure and dynamics of CA-SP1 junction helices in virus-like particles
PNAS, 117 (2020), pp. 10286-10293

12 P.W. Keller, C.S. Adamson, J.B. Heymann, E.O. Freed, A.C. Steven
HIV-1 maturation inhibitor bevirimat stabilizes the immature Gag lattice

J. Virol., 85 (2011), pp. 1420-1428

13 A.J. Pak, M.D. Purdy, M. Yeager, G.A. Voth
Preservation of HIV-1 Gag Helical Bundle Symmetry by Bevirimat Is Central to Maturation Inhibition
J. Am. Chem. Soc., 143 (2021), pp. 19137-19148

14 M.D. Purdy, D. Shi, J. Chrustowicz, J. Hattne, T. Gonen, M. Yeager
MicroED structures of HIV-1 Gag CTD-SP1 reveal binding interactions with the maturation inhibitor bevirimat
PNAS, 115 (2018), pp. 13258-13263

15 W.S. Blair, J. Cao, J. Fok-Seang, P. Griffin, J. Isaacson, R.L. Jackson, et al.
New small-molecule inhibitor class targeting human immunodeficiency virus type 1 virion maturation
Antimicrob. Agents Chemother., 53 (2009), pp. 5080-5087

16 F. Li, R. Goila-Gaur, K. Salzwedel, N.R. Kilgore, M. Reddick, C. Matallana, et al.
PA-457: a potent HIV inhibitor that disrupts core condensation by targeting a late step in Gag processing
PNAS, 100 (2003), pp. 13555-13560

17 J. Zhou, X. Yuan, D. Dismuke, B.M. Forshey, C. Lundquist, K.H. Lee, et al.
Small-molecule inhibition of human immunodeficiency virus type 1 replication by specific targeting of the final step of virion maturation
J. Virol., 78 (2004), pp. 922-929

18 A.B. Kleinpeter, E.O. Freed
HIV-1 Maturation: Lessons Learned from Inhibitors
Viruses, 12 (2020)

19 C.S. Adamson, S.D. Ablan, I. Boeras, R. Goila-Gaur, F. Soheilian, K. Nagashima, et al.
In vitro resistance to the human immunodeficiency virus type 1 maturation inhibitor PA-457 (Bevirimat)
J. Virol., 80 (2006), pp. 10957-10971

20 K. Waki, S.R. Durell, F. Soheilian, K. Nagashima, S.L. Butler, E.O. Freed
Structural and functional insights into the HIV-1 maturation inhibitor binding pocket
PLoS Pathog., 8 (2012), p. e1002997

21 D. Poston, T. Zang, P. Bieniasz
Derivation and characterization of an HIV-1 mutant that rescues IP6 binding deficiency
Retrovirology, 18 (2021), p. 25

22 P.J. French, C.M. Bunce, L.R. Stephens, J.M. Lord, F.M. McConnell, G. Brown, et al.
Changes in the levels of inositol lipids and phosphates during the differentiation of HL60 promyelocytic cells towards neutrophils or monocytes
Proc. Biol. Sci., 245 (1991), pp. 193-201

23 D. Qiu, M.S. Wilson, V.B. Eisenbeis, R.K. Harmel, E. Riemer, T.M. Haas, et al.

Analysis of inositol phosphate metabolism by capillary electrophoresis electrospray ionization mass spectrometry
Nat. Commun., 11 (2020), p. 6035

24 R.A. Dick, K.K. Zadrozny, C. Xu, F.K.M. Schur, T.D. Lyddon, C.L. Ricana, et al.
Inositol phosphates are assembly co-factors for HIV-1
Nature, 560 (2018), pp. 509-512

25 C.L. Ricana, T.D. Lyddon, R.A. Dick, M.C. Johnson
Primate lentiviruses require Inositol hexakisphosphate (IP6) or inositol pentakisphosphate (IP5) for the production of viral particles
PLoS Pathog., 16 (2020), p. e1008646

26 D.L. Mallery, K.M.R. Faysal, A. Kleinpeter, M.S.C. Wilson, M. Vaysburd, A.J. Fletcher, et al.
Cellular IP(6) Levels Limit HIV Production while Viruses that Cannot Efficiently Package IP(6) Are Attenuated for Infection and Replication
Cell Rep., 29 (2019) 3983–96.e4

27 D.L. Mallery, A.B. Kleinpeter, N. Renner, K.M.R. Faysal, M. Novikova, L. Kiss, et al.
A stable immature lattice packages IP(6) for HIV capsid maturation
Sci. Adv., 7 (2021)

28 D.E. Christensen, B.K. Ganser-Pornillos, J.S. Johnson, O. Pornillos, W.I. Sundquist
Reconstitution and visualization of HIV-1 capsid-dependent replication and integration in vitro
Science, 370 (2020)

29 D.L. Mallery, C.L. Márquez, W.A. McEwan, C.F. Dickson, D.A. Jacques, M. Anandapadamanaban, et al.
IP6 is an HIV pocket factor that prevents capsid collapse and promotes DNA synthesis
Elife, 7 (2018)

30 G.A. Sowd, J. Shi, C. Aiken
HIV-1 CA Inhibitors Are Antagonized by Inositol Phosphate Stabilization of the Viral Capsid in Cells
J. Virol., 95 (2021), p. e0144521

31 N. Renner, D.L. Mallery, K.M.R. Faysal, W. Peng, D.A. Jacques, T. Böcking, et al.
A lysine ring in HIV capsid pores coordinates IP6 to drive mature capsid assembly
PLoS Pathog., 17 (2021), p. e1009164

32 T. Ni, Y. Zhu, Z. Yang, C. Xu, Y. Chaban, T. Nesterova, et al.
Structure of native HIV-1 cores and their interactions with IP6 and CypA
Sci. Adv., 7 (2021), p. eabj5715

33 N. Renner, A. Kleinpeter, D.L. Mallery, A. Albecka, K.M. Rifat Faysal, T. Böcking, et al.
HIV-1 is dependent on its immature lattice to recruit IP6 for mature capsid assembly
Nat. Struct. Mol. Biol. (2023)

34 G.A. Sowd, C. Aiken
Inositol phosphates promote HIV-1 assembly and maturation to facilitate viral spread in human CD4+ T cells
PLoS Pathog., 17 (2021), p. e1009190

35 B.G. Luttge, M. Shehu-Xhilaga, D.G. Demirov, C.S. Adamson, F. Soheilian, K. Nagashima, et al.
Molecular characterization of feline immunodeficiency virus budding
J. Virol., 82 (2008), pp. 2106-2119

36 J. Fontana, P.W. Keller, E. Urano, S.D. Ablan, A.C. Steven, E.O. Freed
Identification of an HIV-1 Mutation in Spacer Peptide 1 That Stabilizes the Immature CA-SP1 Lattice
J. Virol., 90 (2016), pp. 972-978

37 E.J. Platt, K. Wehrly, S.E. Kuhmann, B. Chesebro, D. Kabat
Effects of CCR5 and CD4 Cell Surface Concentrations on Infections by Macrophagetropic Isolates of Human Immunodeficiency Virus Type 1
J. Virol., 72 (1998), pp. 2855-2864

38 S.B. Van Engelenburg, G. Shtengel, P. Sengupta, K. Waki, M. Jarnik, S.D. Ablan, et al.
Distribution of ESCRT machinery at HIV assembly sites reveals virus scaffolding of ESCRT subunits
Science, 343 (2014), pp. 653-656

39 R.L. Willey, D.H. Smith, L.A. Lasky, T.S. Theodore, P.L. Earl, B. Moss, et al.
In vitro mutagenesis identifies a region within the envelope gene of the human immunodeficiency virus that is critical for infectivity
J. Virol., 62 (1988), pp. 139-147

40 A.A. Waheed, A. Ono, E.O. Freed
Methods for the study of HIV-1 assembly
Methods Mol. Biol., 485 (2009), pp. 163-184

41 M.A. Checkley, B.G. Luttge, F. Soheilian, K. Nagashima, E.O. Freed
The capsid-spacer peptide 1 Gag processing intermediate is a dominant-negative inhibitor of HIV-1 maturation
Virology, 400 (2010), pp. 137-144

42 D.N. Mastronarde
Automated electron microscope tomography using robust prediction of specimen movements
J. Struct. Biol., 152 (2005), pp. 36-51

43 W.J.H. Hagen, W. Wan, J.A.G. Briggs
Implementation of a cryo-electron tomography tilt-scheme optimized for high resolution subtomogram averaging
J. Struct. Biol., 197 (2017), pp. 191-198

44 S.Q. Zheng, E. Palovcak, J.P. Armache, K.A. Verba, Y. Cheng, D.A. Agard

MotionCor2: anisotropic correction of beam-induced motion for improved cryo-electron microscopy
Nat. Methods, 14 (2017), pp. 331-332

45 D.N. Mastronarde, S.R. Held
Automated tilt series alignment and tomographic reconstruction in IMOD
J. Struct. Biol., 197 (2017), pp. 102-113

46 B.A. Himes, P. Zhang
emClarity: software for high-resolution cryo-electron tomography and subtomogram averaging
Nat. Methods, 15 (2018), pp. 955-961

47 T. Ni, T. Frosio, L. Mendonca, Y. Sheng, D. Clare, B.A. Himes, et al.
High-resolution in situ structure determination by cryo-electron tomography and subtomogram averaging using emClarity
Nat. Protoc., 17 (2022), pp. 421-444

48 J. Ning, G. Erdemci-Tandogan, E.L. Yufenyuy, J. Wagner, B.A. Himes, G. Zhao, et al.
In vitro protease cleavage and computer simulations reveal the HIV-1 capsid maturation pathway
Nat. Commun., 7 (2016), p. 13689